First report about the commissioning of the new Effelsberg sub-reflector

U. Bach, A. Kraus, E. Fürst, and A. Polatidis

Max-Planck-Institut für Radioastronomie Bonn

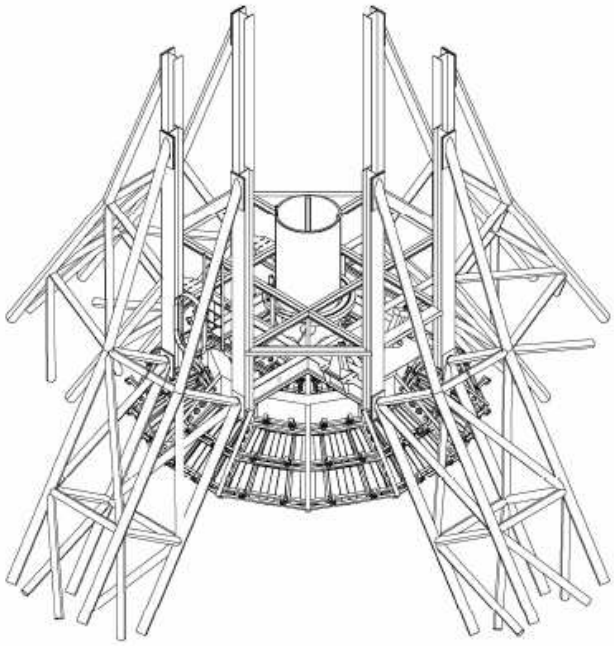

Version of September 11, 2007

CONTENTS

LIST OF FIGURES

LIST OF TABLES

Chapter 1

Introduction

On October 5, 2006 a new sub-reflector equipped with an adjustable surface was mounted on the 100 m Effelsberg telescope. The higher accuracy of its panels shall increase the sensitivity at the higher frequencies in the secondary focus and the elevation dependent adjustment of the surface is supposed to minimize the gain dependence on elevation.

Since the hexapod now allows to adjust the sub-reflector in all three lateral and rotational directions and the exact position of the new system might differ from the old configuration, new focus curves had to be measured for all receivers. The hexapod control of the sub-reflector became fully functional in November 2006. The control of the active surface is used since January 2007. So far the active surface is controlled by a predefined matrix with position entries for all 96 actuators for steps in elevation of 0, 10, 20, 30, 32, 40, 50, 60, 70, 80, and 90 degrees. The matrix was delivered by MT Mechatronics (also known as MAN and MT Aerospace) and is based on a FE model of the gravitational deformation of the main-dish. Holographic measurements to verify or improve the model are currently discussed.

This document describes the testing phase, commissioning, and the calibration of the new system with all secondary and some of the primary focus receivers. A description of the new system is given in Sect. 2, and the focus and calibration measurements are shown in Sect. 3. Open points which need further testing are discussed in Sect. 4. This section includes also a comment about the new focus formulas that were introduced when this report was already finished. The consequences of this modification are not completely clear yet and will be described in a second report (Bach et al. in perp.). A more detailed description of the individual measurements, which were used to obtain the new focus curves are given in the Appendix.

Acknowledgements We thank J. Neidhöfer, P. Müller, T. P. Krichbaum, and W. Reich for discussions and suggestions that helped to perform and interprete the test observations. In particular we like to thank J. B. Schraml for noticing the need for new focus formulas.

Chapter 2

The New Sub-Reflector

The basic parameters of the new sub-reflector are equal to the ones of the old one. It has a radius of 3.25 m and an elliptical shape with a major axis of 14.305 m and a minor axis of 7.3872 m. The two foci are therewith at about 2.055 m and 28 m separated from the vertex of the sub-reflector. One of the major improvements of the new sub-reflector is the higher accuracy of its surface. The surface rms is only $\sim 60\,\mu$m with respect to a perfect elliptical reflector whereas the old surface showed a rms of $\sim 800\,\mu$m.

The new sub-reflector is mounted to the prime focus cabin with a hexapod which allows the adjustment of all three lateral and rotational axes (see Tab. 2.1). In comparison, the old system was only adjustable linearly along the optical axis, and along the elevation direction and rotatable around the elevation axis. The new degrees of freedom and the larger movable ranges should allow to better illuminate secondary receivers further away from the optical axis and to use multi-frequency receiver boxes with up to four different receivers to be positioned in the prime focus.

The correspondence of the old focus curves, FCs, and the hexapod axes[1] are:

$$FC1 = -x_{\mathrm{lin}} + 12 \tag{2.1}$$

$$FC2 = -z_{\mathrm{lin}} - 50 \tag{2.2}$$

$$FC3 = y_{\mathrm{rot}} \tag{2.3}$$

In the following we will only use the new notations of the hexapod axes. In Table 2.1 the possible driving ranges of the hexapod mount are given. A little sketch of the hexapod coordinate system is shown in Fig. 2.1. The coordinate system is a right handed system. The figure also shows that movements along the x-axis correspond to shifts along the elevation direction, where positive values correspond to shifts towards lower elevations and the y-axis corresponds to movements along the azimuth direction, where positive shifts steer the sub-reflector towards the B-tower.

Another advantage of the new sub-reflector is the possibility to change from secondary to prime focus observations within a few minutes using the control panel in the control room. The telescope has to be pointed at least to 88 degrees elevation, then the receiver which is actually present in the prime focus tube can be brought into the focus or pulled back. The receiver has to be filled in to the prime focus tube by hand; three receivers

[1] The offset of 12 mm was measured during the preparations for the new sub-reflector and marks the offset of the old reflector with respect to the centre of the prime focus cabin. An offset of 16 mm was measured for y_{lin}. In addition a slope in x_{rot} of 27 arcmin was noted.

can be stored and kept cool in the prime focus cabin. New prime focus boxes are build, which might carry up to four different frequency receivers which will again increase the frequency flexibility of the Effelsberg telescope. A first dual box (1.0/1.9 cm) was already successfully tested (see Sect. 3.2 for more details).

Table 2.1: Properties of the hexapod mount. Given are the name of the focus axis in the telescope control software, the corresponding axis of the hexapod control (see also Fig. 2.1), the minimum and maximum drivable ranges. "pol" means the rotation of the polarization angle around the z-axis, which is a independent system from the hexapod and therewith from z_{rot}. The new "pol" angle has an offset of $-90°$ to the old definition. Viewed from the secondary focus a positive rotations direction corresponds to a clockwise rotation.

Old Name	Axis	min [mm (°)]	max [mm (°)]
FC1	x_{lin}	-230	$+230$
	y_{lin}	-180	$+180$
FC2	z_{lin}	-200	$+100$
	x_{rot}	(-1.0)	$(+1.0)$
FC3	y_{rot}	(-1.0)	$(+1.0)$
	z_{rot}	(-0.2)	$(+0.2)$
pol	pol	(-195)	(195)

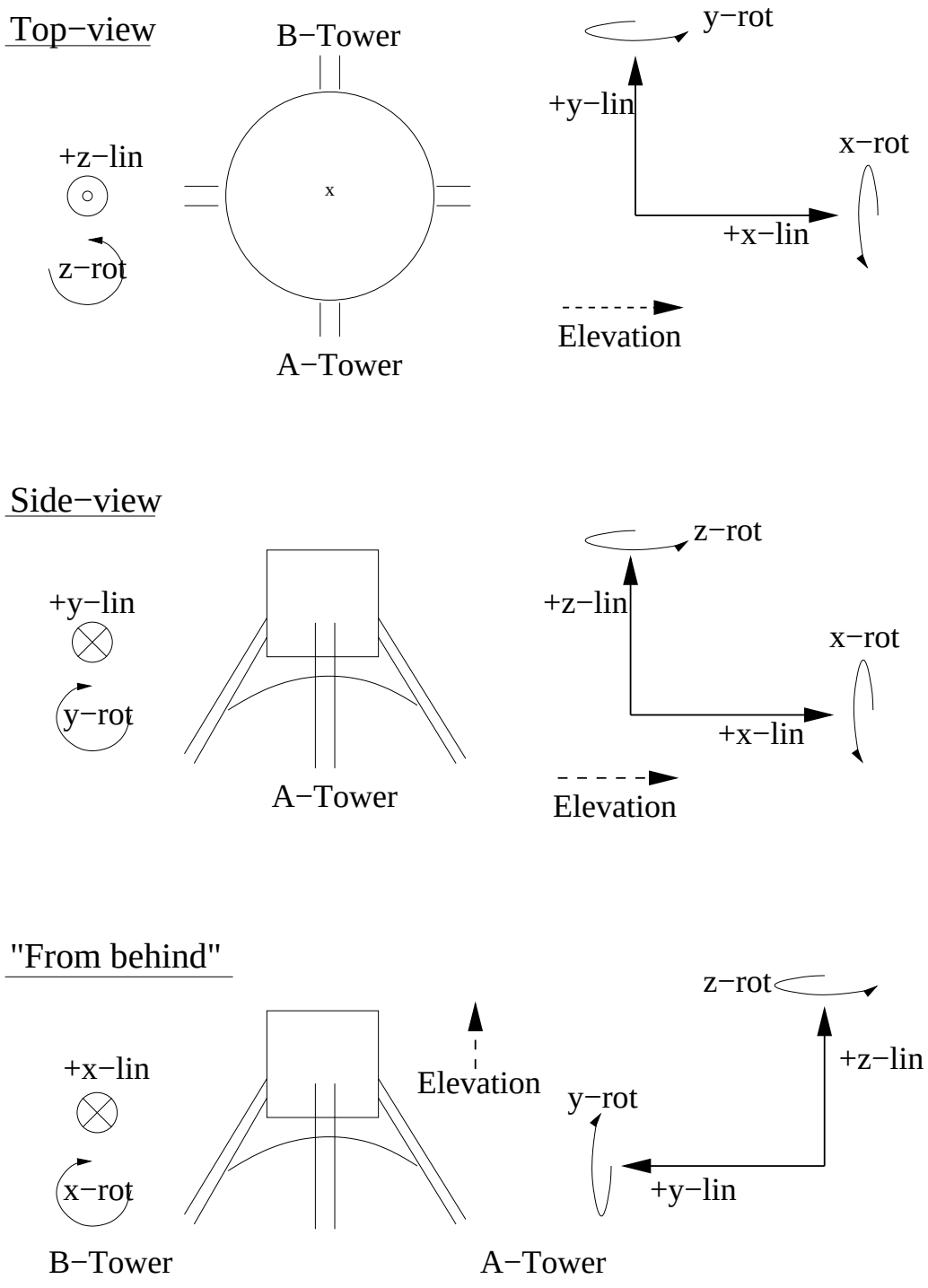

Figure 2.1: Coordinate system of the Hexapod.

Chapter 3

Improvements

3.1 Secondary Focus

Most of the test are done and for all of the secondary focus receivers new focus and gain curves have been measured. We first present the new advantages in terms of higher sensitivity and improved gain curves and later describe the measurement of the new focus curves.

3.1.1 Sensitivities and Gain Curves

The surface-rms for the secondary focus is a combination of the rms of the main dish and the rms of the sub-reflector. The theoretical sensitivity, Γ, for a specific wavelength, λ, can be calculated by the Ruze formula:

$$\begin{aligned} \Gamma &= \eta_{\mathrm{A}} \cdot \Gamma_0 = \eta_{\mathrm{A}} \cdot \frac{A_{geom}}{2\mathrm{k}} = \eta_{\mathrm{A}} \cdot \frac{\pi D^2}{8\mathrm{k}} = \eta_{\mathrm{A}} \cdot 2.844 \text{ K/Jy} \qquad (3.1) \\ \text{with} \quad \eta_{\mathrm{A}} &= \eta_0 \cdot \exp\left(-0.78 \cdot \left(\frac{4\pi\sigma}{\lambda}\right)^2\right) \quad \text{and} \quad \sigma = \sqrt{\sigma_{\mathrm{P}}^2 + \sigma_{\mathrm{S}}^2}, \end{aligned}$$

where η_{A} is the aperture efficiency, k the Boltzmann constant, A_{geom} the geometric area of the antenna, and σ_{P} and σ_{S} the rms of the primary and secondary mirror. Using $\eta_0 = 0.55$, $\sigma_{\mathrm{P}} = 0.55\,\mathrm{mm}$, $\sigma_{\mathrm{S,old}} = 0.75\,\mathrm{mm}$, and $\sigma_{\mathrm{S,new}} = 0.1\,\mathrm{mm}$ the higher accuracy of the sub-reflector surface should increase the sensitivity at 10 GHz from 1.37 K/Jy to 1.47 K/Jy.

The old and new sensitivities are given in Table 3.1. An obvious increase is visible at all wavelength specially at the higher frequencies above 8 GHz. However, for e.g, 32 GHz a sensitivity of about 1.0 K/Jy would be expected from the surface rms, but it is currently not reached. Further test to solve this discrepancy are planned (see Sect. 4).

The active surface of the new sub-reflector shall be able to compensate, at least to some extend, the known deviations of the main dish from the perfect paraboloid and the gravitational deformations which appear above and below elevations of 32 degrees. At this elevation the panels of the main dish were adjusted by holography and should provide an rms of about 0.55 mm (e.g., Kesteven et al. 2001; Reich & Fürst 1999).

In Figure 3.1 the current aperture efficiency as a function of elevation at 9 mm is compared with the theoretical prediction, which was simulated during the planing phase

Table 3.1: Characteristics of SFK receivers. Given are the beam size, the old sensitivity, the theoretical new sensitivity (using $\sigma_P = 0.55$ mm and $\sigma_{S,new} = 0.1$ mm), the measured new values, and the improvement in percentage.

RX	Beam [″]	Old sens. [K/Jy]	Theo. sens. [K/Jy]	New sens. [K/Jy]	Improv. [%]
110	265.3	1.55	1.56	1.57	1
60	147.8	1.55	1.55	1.57	1
36	82.8	1.28	1.52	1.37	7
28	67.6	1.30	1.49	1.47	13
20	50.9	1.05	1.43	1.15	10
13	36.0	0.80	1.25	0.86	7
9	26.2	0.45	1.01	0.66	47
7	20.3	0.35	0.72	0.45	29

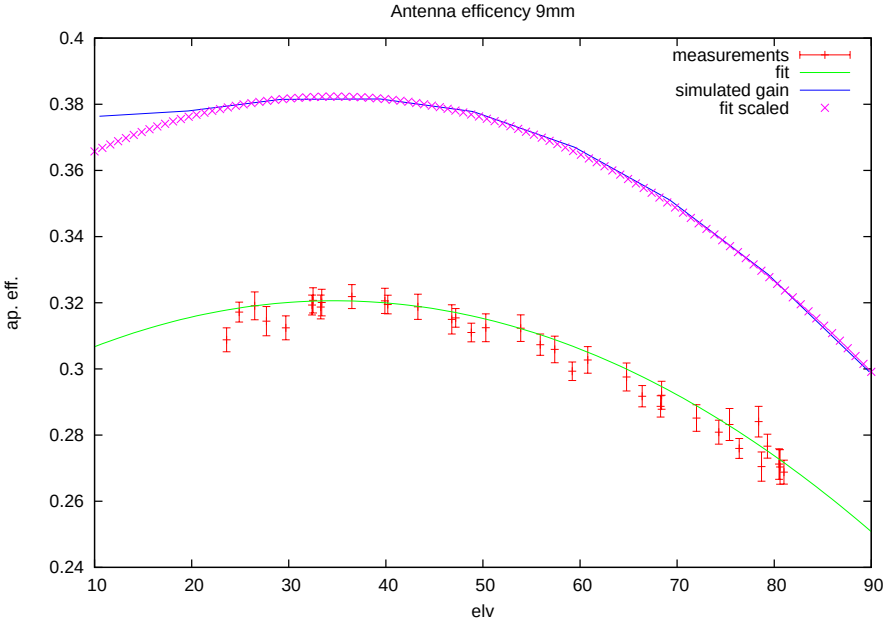

Figure 3.1: Predicted and measured gain-elevation dependence. The shapes of the two curves agree perfectly, but the current observed efficiency is about 15% lower than expected.

of the new system. As mentioned above, the total efficency is a bit lower than expected, but the trend with elevation is exactly as it was expected. This proves that the current matrix, which controls the sub-reflectors active surface compensates quite well the known problems of the main dish. However future holographic measurements at different elevations would be desirable to image the residual surface errors in order to improve the lookup table.

Examples of the new gain curves are shown in Figures C.9 & C.11 (p. 23 ff). A comparison between all the gain curves together can be found in Figure 3.2. *The 6 cm gain curve displays a strange increase below 20 degrees elevation, which is so far not understood (see also Sect. 4).*

3.1.2 Focus curves

The new degrees of freedom and the many changes (e.g., axis offsets) that were introduced with the installation of the hexapod drive required new measurements of the focus curves that control the proper focusing of the telescope. The main contributions to the focus curves come from the homology and bending of the telescope structure. In Figure 3.3 a

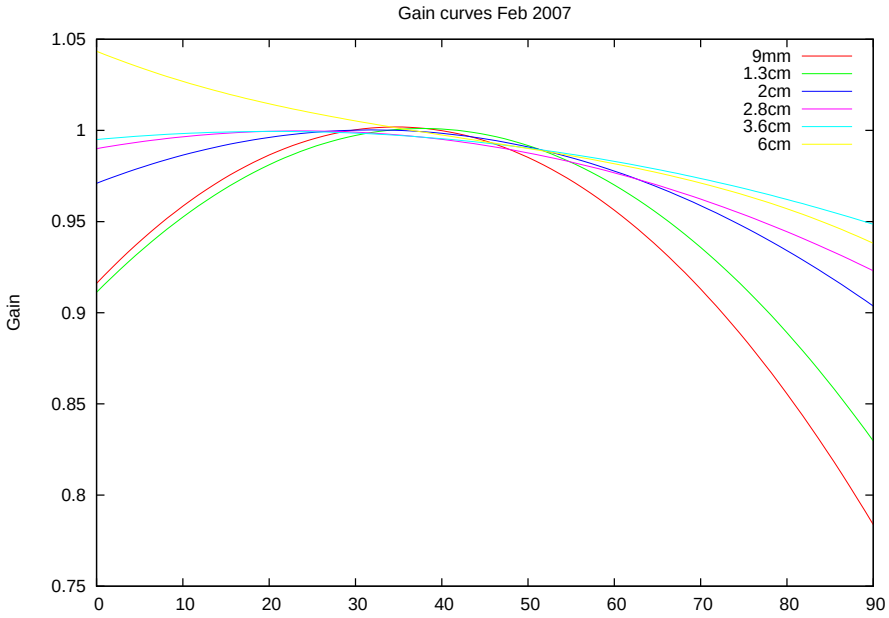

Figure 3.2: New gain curves SFK.

comparison of the new and old focus curves is shown. There is obviously an offset in x_{lin} which can be easily understood as a position offset between the mounting or the coordinate system of the old and the new sub-reflector. Measurements of the exact position of the old sub-reflector with respect to the prime focus cabin by MT Mechatronic in 2005 revealed an offset of about 12 mm in x for the zenith position of the telescope. This is comparable with the value obtained by the astronomical measurements.

More curious seems to be the different slope in x_{lin}. Several possibilities could be responsible for the new shape:

1. The focus curves were not checked since 30 years and the changes could have been already there before but were never measured.

2. We still have an undetected offset or different slope for the tilt vs. elevations of the sub-reflector, which is now compensated by the radial shift.

It should be possible to check all points with the ongoing measurements of the focus curves for the prime focus receivers. The "advantage" of the primary focus is that the positions there should be independent of the tilt around the axes. We can therefore work with only three variables, x_{lin}, y_{lin}, and z_{lin} (see Figure 2.1). In addition the position in y_{lin} should be independent of the elevation.

After measuring the prime focus curve for x_{lin} it should be possible to use this x_{lin}-curve also for the secondary focus and adjust only the residual elevation dependence using the tilt, y_{rot}. In the same manner the y-position of the prime focus can be used to adjust x_{rot} once for the receivers close to the optical axes. Afterwards the y-position can be adjusted for the receivers further off the optical axis (3.6, 2, 1.3, and 0.7 cm). More details about the prime focus measurements can be found in Sect. 3.2 (p. 8). The formulas to calculate the focus positions are as follows:

$$
\begin{aligned}
y_{\text{rot}} &= F6 \cdot \cos(ELV) \\
-x_{\text{lin}} &= F1 \cdot \cos(ELV) + F2 - 1961 \cdot (1 - \cos(y_{\text{rot}})) - 3290 \cdot \sin(y_{\text{rot}}) \\
-z_{\text{lin}} &= F3 \cdot \cos(ELV) + F4 \cdot \sin(ELV) + F5 \\
&\quad +1961 \cdot \sin(y_{\text{rot}}) + 3290 \cdot (1 - \cos(y_{\text{rot}}))
\end{aligned}
$$

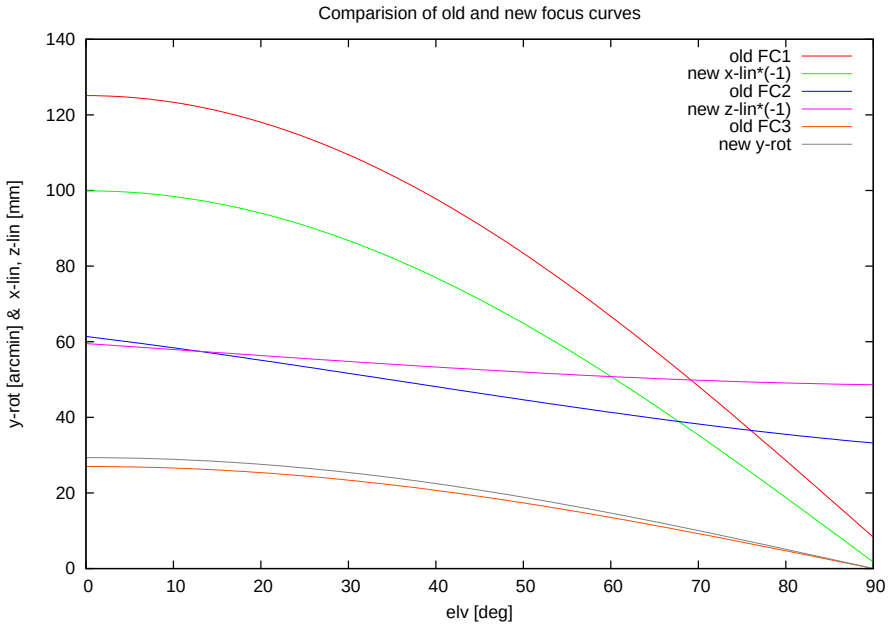

Figure 3.3: Comparison of the new and old focus curves. Please note that the new curves have a different sign and are multiplied by (-1) to allow a better comparison.

The parameters $F1$ to $F6$ for all receivers are given in Table A.1 (p. 14). The different slope of z_{lin} can be mostly attributed to the change of the x_{lin} slope. The present y_{rot} curve does not significantly differ from the old one, but a small offset was introduced at some point because measurements done with a small positive offset appeared marginally better. If this offset is correct should be verified by measurements using the prime focus x_{lin} curve. *In the mean time, when this report was already finished, new focus formulas were introduced by J. Schraml. The new formulas consider that the point around that the rotations are performed is now located in the vertex of the sub-reflector and not at the frame, as for the old one. Therewith the* $(1-\cos(y_{\text{rot}}))$ *and* $sin(y_{\text{rot}})$ *terms have changed, but the consequences of this modification are not completely clear yet and will be described in a second report (Bach et al. in prep.). The new formulas are show in Sect. 4.*

In Figure 3.4 a comparison of all x_{lin} SFK receiver curves can be found. The old system had only two curves with slightly different slopes for high and low frequencies. "High" and "low" was distinguished at 5 GHz. Since no common x_{lin} focus curve could be found for all high frequency receiver above 10 GHz individual curves were measured for every receiver. The trend is the same as with the old curve that towards higher frequencies the x_{lin} curves appear flatter at high elevations. The offsets are due to the different positions of the receivers in the secondary focus cabin. The measured offsets with respect to the 2.8 cm receiver are listed in Table 3.2. The z_{lin} offsets are due to differences in the hight on the receiver in the prime focus cabin. The receiver dependent changes of x_{lin} and y_{lin} scale as $\sim 0.005 * \theta$ mm, where θ is the angle of the positions of the specific receiver from the 2.8 cm receiver seen from the prime focus cabin in arcseconds. We note that this is ongoing work and some of these numbers have to be considered as preliminary. More details will be given in the second report.

3.2 Primary Focus

Since prime focus receivers will "see" the main dish directly a sensitivity improvement or a better gain elevation dependence is not expected for prime focus observations. Nevertheless a better performance might be reached due to the possibility of adjusting the receiver in

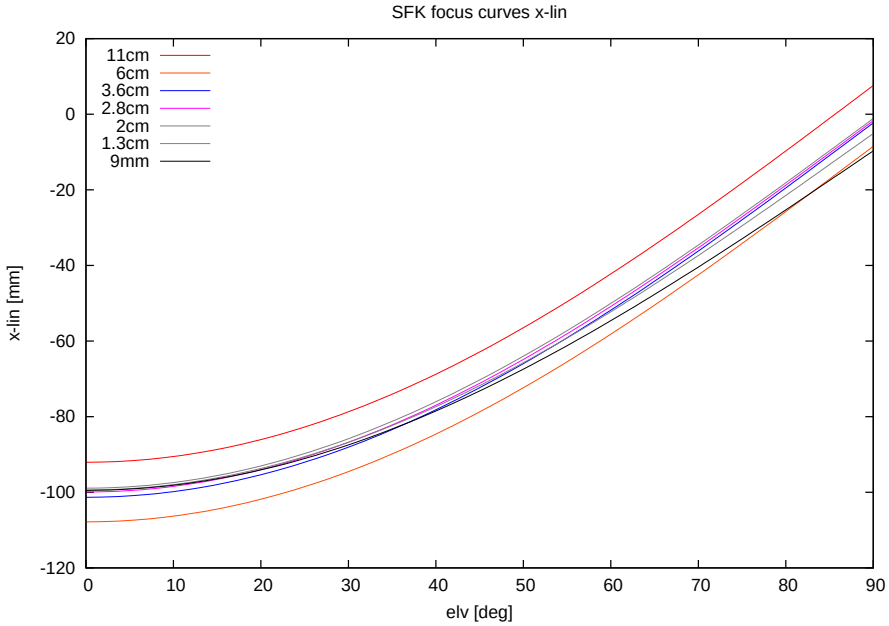

Figure 3.4: Comparison of the new x_{lin} focus curves for all secondary focus receivers.

Table 3.2: Measured offsets between secondary focus receivers.

RX	x_{lin} [mm]	z_{lin} [mm]	y_{lin} [mm]
07	−2.0	−0.4	−2.0
09	−5.0	−0.2	0.0
13	−2.0	−0.2	−3.0
20	−2.0	−0.2	−4.0
28	0.0	0.0	0.0
36	−0.5	−2.0	3.0
60	5.0	−27.0	0.0
110	−11.0	−22.0	0.0

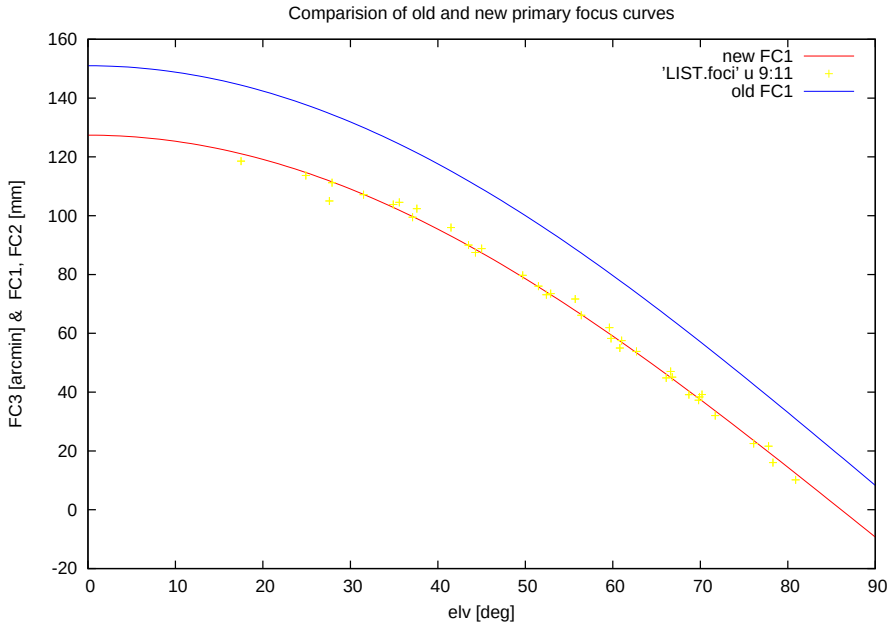

Figure 3.5: Comparison of old and current prime focus curves.

y_{lin} (azimuth direction) and a clear advantage will be the installation of three or four receiver boxes which will increase the frequency flexibility for prime focus observations.

So far, in the prime focus the different receivers are not all available at the same time. The primary focus tube can be loaded with one receiver box which then can be driven into its focus position automatically from the control room. This allows to switch from secondary to primary focus observations within a few minutes. The only restriction is that the telescope has to be pointed at least to 88° elevation. With the newly build receiver boxes up to four different frequency receivers will fit into the prime focus tube allowing a more flexible scheduling of different projects. With this it will be possible to choose between up to 13 different receivers (9 secondary and 4 primary ones), which are available constantaneous.

First measurements were done at 18 and 21 cm and despite some constant offsets in x_{lin} and z_{lin}, which agree with the offsets found in the secondary focus, no changes were found to the previous focus curve. Given the low resolution at this long wavelength this was not surprising. The tilt, y_{rot}, is constantly zero for all prime focus observations.

Further measurements were done at 5 cm and 1.3 cm. The old and the new x_{lin} focus curves are compared in Figure 3.5. The offset is comparable to the secondary focus curve, but the slope did not flatten as much as for the prime focus receivers. This could be a hint that we need to introduce an offset for the y_{rot} curve (y_{rot}) for the secondary focus curves. With that we could probably bring the primary and secondary x_{lin} curves in agreement.

The 1.3 cm receiver is a beam switch system where the two horn positions are separated by about 25 arcsec in azimuth direction. So far this position was fixed, because the old reflector was not movable along the azimuth direction. With the hexapod system we are able to move the main horn closer to the optical axis, resulting in an increase of the sensitivity by about 10 % (see Fig. 3.6).

3.2.1 Multi-Receiver Boxes

The first multi-receiver boxes which could be tested was the 1.0/1.9cm box. A new 21/18cm receiver will be included in this box later. Since the horns are not located at the centre (optical axis) the box has to be rotated and positioned in x_{lin} and y_{lin} in a way that the positions of the focus curve in x_{lin} will never contradict with the driving limits of the

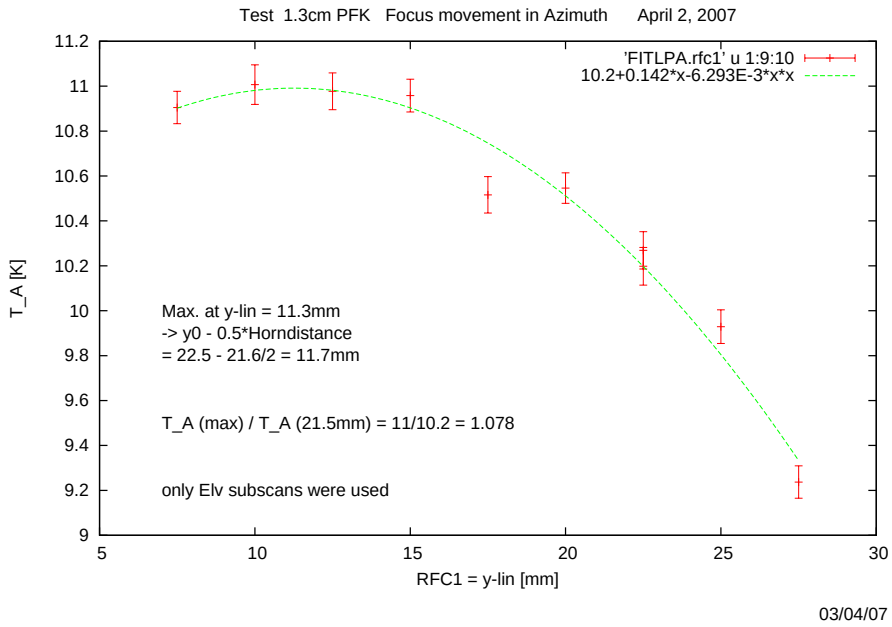

Figure 3.6: Measurements at 1.3cm testing different focus positions along the azimuth axis.

hexapod. The limits are at $x_{\rm lin}$= ±230 mm and $y_{\rm lin}$ = ±180 mm and the distances of the receivers from the optical axis are about 260 mm with offsets of about 100 mm in x and 240 mm in y. Since the polarization rotation mechanism is used to perform the rotation the consequence is that during observations with the multi-receiver boxes the polarization angle has to be kept fixed. The values for the rotation of the polarization angle (pol), $x_{\rm lin}$ and $y_{\rm lin}$ which were found during the first test and which fullfill all the requirements for the positions in $x_{\rm lin}$ and $y_{\rm lin}$ are given in Table 3.3

Table 3.3: Positional parameters to bring different horns of the dual-frequency box (1.0/1.9 cm) in to the prime focus position. The 18 cm receiver is so far not integrated into the receiver box and therefore the given postions are "only" calcuated values.

RX	pol [°]	$x_{\rm lin}$ [mm]	$y_{\rm lin}$ [mm]
1.0 cm	340	−226.1	165.0
1.9 cm	68	−223.8	174.0
18 cm	218	−203.8	170.0

Chapter 4

Remaining questions

1. Although the 9 mm sensitivity has improved a lot, why do the other secondary focus receivers above 2.8 cm do not show the expected increase in sensitivity?
2. Why is the sensitivity at 3.6 cm lower than at 2.8 cm? Can the 3.6 cm sensitivity be increased by further adjusting y_{lin}.
3. What causes the strange increase of the 6 cm gain curve towards elevations below 20°?
4. Can the position matrix of the active surface be improved?
5. It was noticed that the foci change with the active surface being on or off. It should be tested if we could provide two sets of focus constants depending on the status of the active surface.

The first two points might improve by a further adjustment of the sub-reflector in y_{lin} and x_{rot}. Some of the problems might have been solved during finishing this report. J. Schraml found out that the old focus formulas include correction terms for the tilt in elevation that were special for the mechanic realisation and the geometry of old sub-reflector and are not appropriate anymore. Since the tilt around one of the focus axes has still an effect on the primary focus point which has to be aligned with the focal point of the main dish, corrections are still needed, but the formulas have changed. The new formulas have the following form:

$$y_{\mathrm{rot}} = F6 \cdot \cos(ELV) \tag{4.1}$$

$$-x_{\mathrm{lin}} = F1 \cdot \cos(ELV) + F2 - 2055 \cdot \sin(y_{\mathrm{rot}}) \tag{4.2}$$

$$-z_{\mathrm{lin}} = F3 \cdot \cos(ELV) + F4 \cdot \sin(ELV) + F5 - 2055 \cdot (1 - \cos(y_{\mathrm{rot}})) - 2055 \cdot (1 - \cos(x_{\mathrm{rot}})) \tag{4.3}$$

The parameters $F1$ to $F6$ for all receivers have been re-measured recently with the new formulas. The results with the new focus curves and their consequences will be presented in a second report (Bach et al. in prep.).

BIBLIOGRAPHY

Kesteven, M., Graham, D., Fürst, E., Lochner, O., & Neidhöfer, J. 2001, The Effelsberg Holography Campaign - 2001, Effelsberg Memo, http://www.mpifr-bonn.mpg.de/div/effelsberg/advanced_points.html

Reich, W. & Fürst, E. 1999, Kleinheubacher Berichte

Appendix A

Focus Parameters

Table A.1 gives all the individual values that were measured for the focus parameters shown in the equations on page 6.

Table A.1: Focus parameters for different receivers (from Sept. 2007).

RX	$F1$ [mm]	$F2$ [mm]	$F3$ [mm]	$F4$ [mm]	$F5$ [mm]	$F6$ [arcmin]
			secondary focus			
110	105.8	−13.6	2.6	−9.0	30.3	27.0
60	105.8	2.4	2.6	−9.0	27.1	27.0
36	105.8	−2.6	2.6	−9.0	50.0	27.0
28	103.3	−0.3	2.6	−9.0	54.9	27.0
20	98.5	2.1	2.6	−9.0	52.0	27.0
13	95.7	4.4	2.6	−9.0	54.5	27.0
09	88.4	8.4	2.6	−9.0	51.3	27.0
07	86.7	12.9	2.6	−9.0	52.4	27.0
			primary focus			
all	138.4	−15.9	−0.3	−15.0	150.7	0

Appendix B

Active Surface

Figure B.1 shows the adjustment of the sub-reflector panels which should compensate for the deformations that appear in the main dish. The values are read by the control system from a look up table provided by MT Mechatronics. Fine tuning of the adjustments using test observations with modified look up tables or holographic observations are planed for the near future.

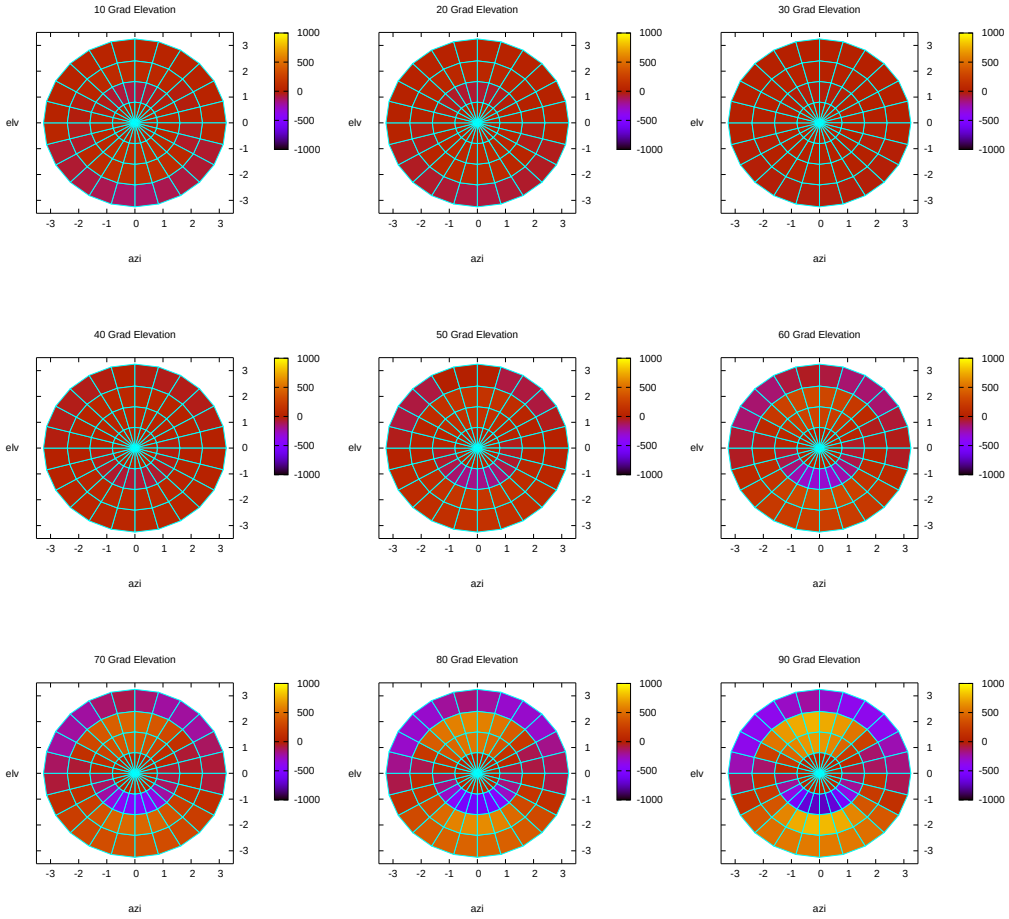

Figure B.1: Shown are the positions of the sub-reflector panels in microns for different elevations starting from 10° (top-left) to 90° (bottom-right). The main dish is optimized for 32° and therefore deviations appear mainly and much lower and much larger elevations.

Appendix C

Observations

This section summarizes the performed observations, which were necessary to obtain the new focus curves.

C.1 Update of old Focus Curves

The first measurements were done without any automatic control of the focus positions and the focus was adjusted by hand using the old tabulated focus curves for 5 degrees steps on elevation. An example how de-focused cross scans look like is given in Figure C.1.

In Figure C.2 another strongly de-focused 9 mm scan is shown. At some point in addition to the coma also a noticeable deviation from a Gaussian profile is visible.

Since the pointing depends strongly on the radial focus parameters the first adjustments were all done by hand. For this, bright sources were tracked for a long time over many different elevations and the focus parameters were changed until a symmetric profile was found. Additional parameters to judge over the best focus parameters were obviously the amplitude and the width of the cross scan. However for shorter wavelength where the cross scan results depend more strongly on elevation and weather the direct comparison of scans becomes more difficult. With the resulting rough focus curves and the adjustment of the pointing model to this curves, automatic procedures could be used to obtain more accurate focus curves. Automatic focus procedures exist for x_{lin}, z_{lin}, and y_{rot}, and are called: focus, rfocus, and kfocus respectively. The focus and rfocus procedures work quite well but the kfocus for the tilt is very insensitive and requires large driving ranges, which is again problematic since the tested focus position could be off source and the compared focus position correspond just to the noise left and right of the source.

In addition to the cross scans, beam calibration maps were done. The maps allow a closer examination of the symmetry of the beam pattern. Long sequences of calibration maps for various offsets for the different focus parameters were done around our best fit models from the cross scans and on most cases the symmetry was already very good. Examples of beam calibration maps are given in Figure C.3.

C.2 New Parameters

The control of the focal position along the azimuth direction is a new degree of freedom. The old sub-reflector was fixed in this direction. Figure C.4 shows a test for various positions along the radial azimuth shift y at 5 cm from the prime focus. The advantage of focal measurements from the prime focus is that the tilt of the sub-reflector is negligible.

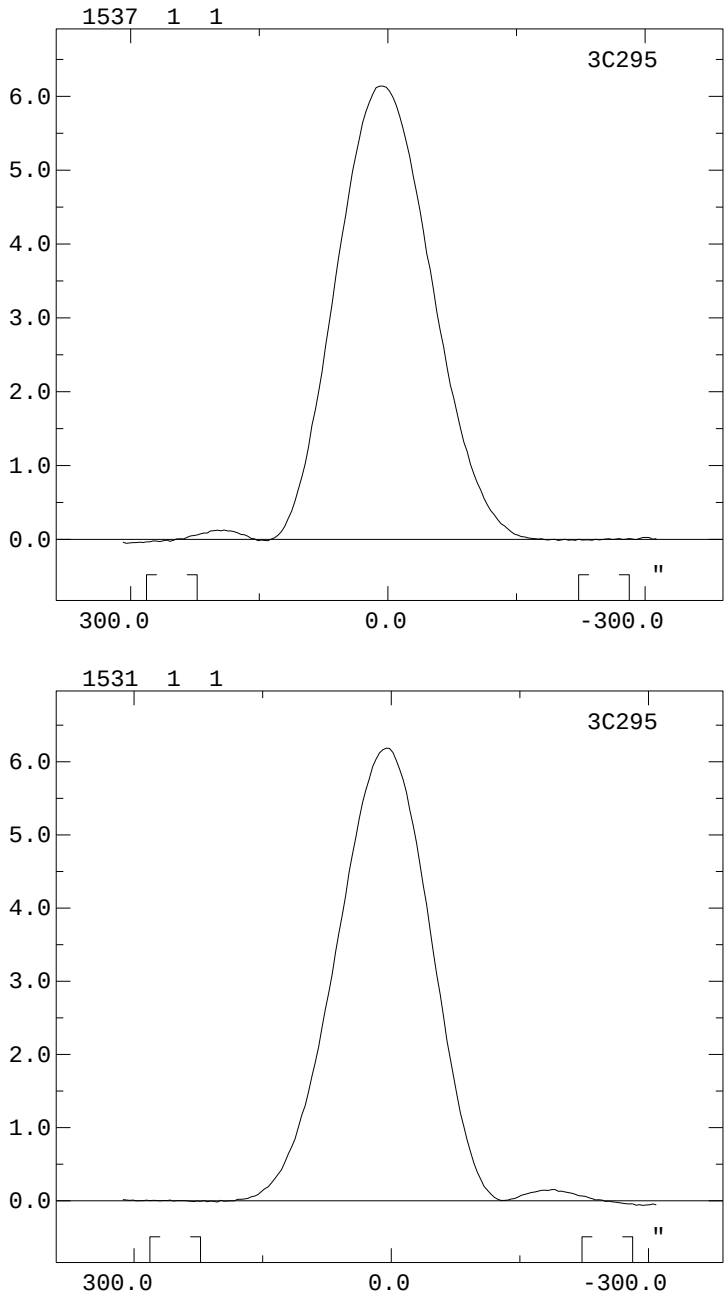

Figure C.1: Two radial de-focused cross scans in azimuth. Depending on the direction of the de-focusing a coma appears left or right of the main beam. **Top:** Taken with a too high value for y_{lin}.**Bottom:** Taken with a too low value for y_{lin}.

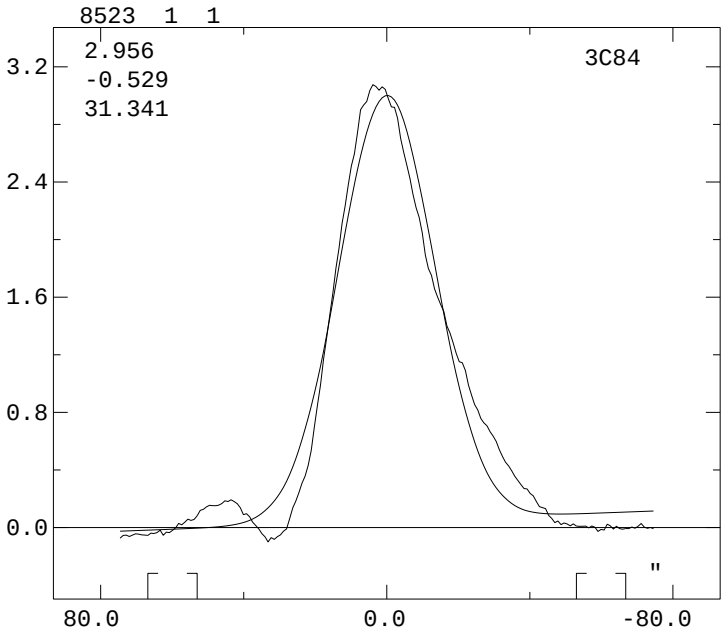

Figure C.2: Strongly de-focused elevation scan. Not only the coma but also a clear deviation from the Gaussian profile is also visible.

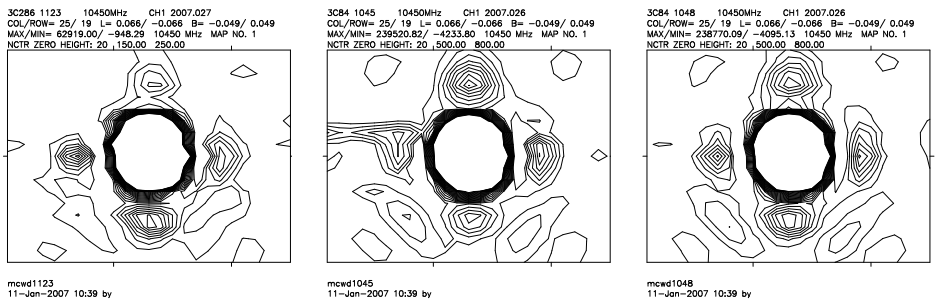

Figure C.3: Three calibration maps obtained at different elevation and with different SFC1 offsets. **Left:** 3C 286 at 62° elevation and SFC1 = 8. The southern side lobe seems stronger, which means that the offsets is too large. **Middle** 3C 84 at 78° elevation and SFC1 = 0. The northern side lobe appears stronger, which means that the offsets is too small. **Right:** 3C 84 at 76° elevation and SFC1 = 4; looks quite symmetric.

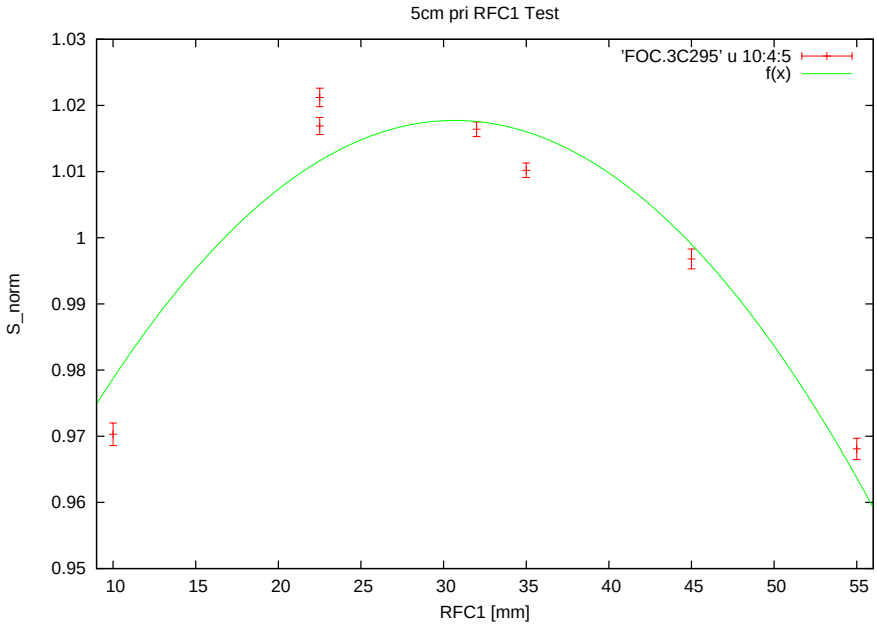

Figure C.4: Relative amplitude of cross scans taken at different y_{lin} positions at 5 cm (prime focus).

Figures C.5 & C.6 show measurements at 3.6 cm and 2 cm which were performed to find the optimal combination of y_{lin} and x_{rot} to better illuminate the receivers further away from the optical axis of the secondary focus. There is a measurable increase at both frequencies: The best value for 3.6 cm for a constant x_{rot} of 17 arcmin seems to be $y_{\mathrm{lin}} = 26$ mm and at 2 cm $y_{\mathrm{lin}} = 19$ mm. The current default is 22.5 mm.

C.3 Multi-Frequency Boxes

Figures C.7 & C.8 show the test observations which were done to position the 1.9 cm receiver of the new prime focus multi-frequency box along the optical axis. In an iterative process the x_{lin} and y_{lin} positions were adjusted and a polarization rotation was performed to avoid possible conflicts with the driving range limits of the hexapod.

C.4 New Gain Curves

As two examples the gain curves and sensitivities of the 9mm and the 2.8cm secondary focus receivers are shown (Fig. C.9 to C.12). The other gain curves can be found on the Effelsberg web pages (see `http://www.mpifr-bonn.mpg.de/div/effelsberg/receivers/receiver.html`).

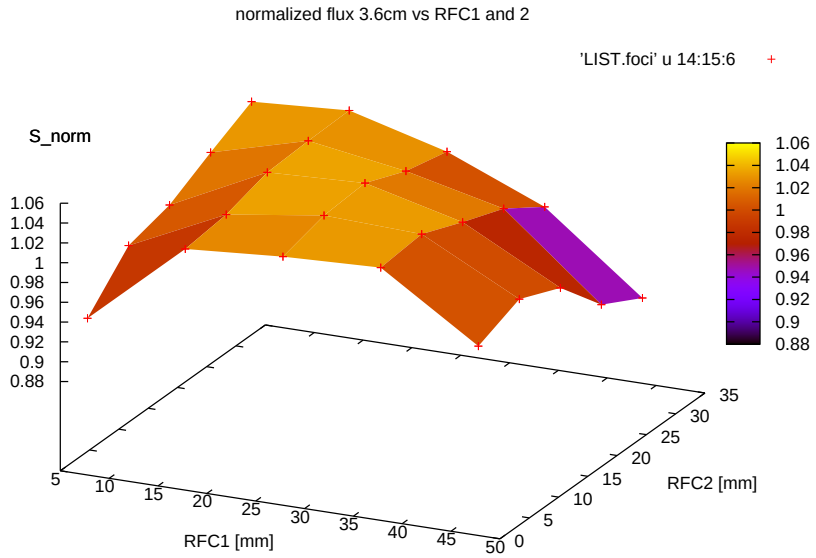

Figure C.5: Relative amplitude of cross scans taken at different y_{lin} and x_{rot} positions for 3.6 cm.

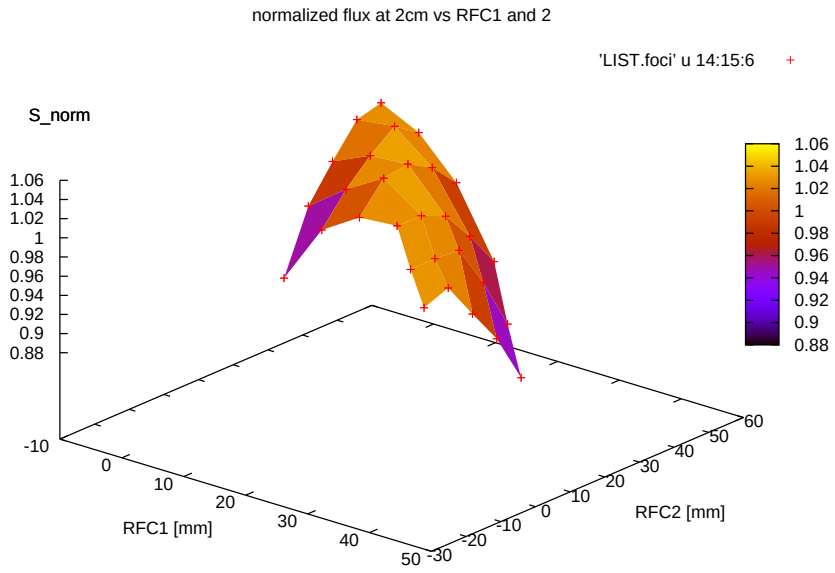

Figure C.6: Relative amplitude of cross scans taken at different y_{lin} and x_{rot} positions for 2 cm.

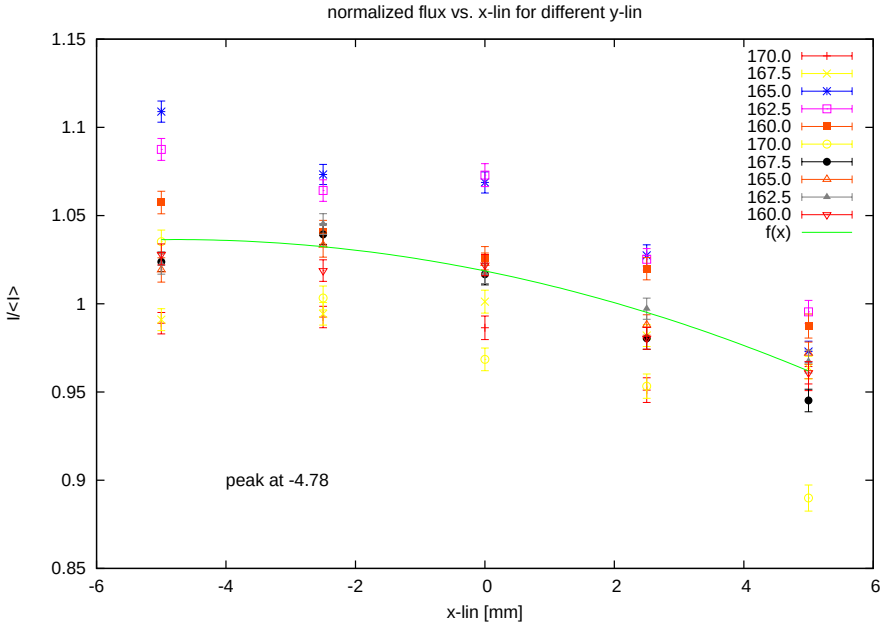

Figure C.7: Relative amplitude of cross scans taken at different x_{lin} and y_{lin} positions to optimize the position of the 1.9 cm receiver from the multi-frequency box at the prime focus.

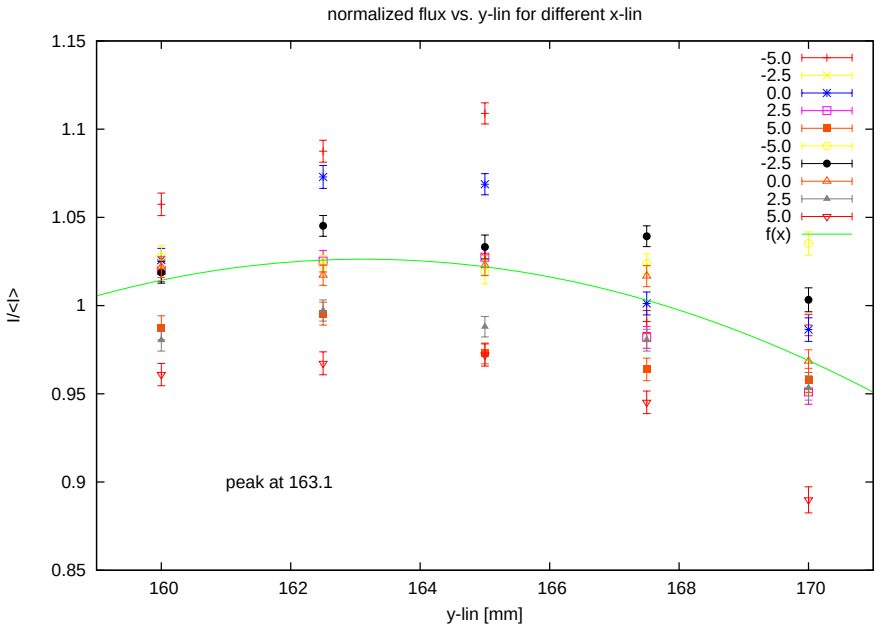

Figure C.8: Relative amplitude of cross scans taken at different x_{lin} and y_{lin} positions to optimize the position of the 1.9 cm receiver from the multi-frequency box at the prime focus.

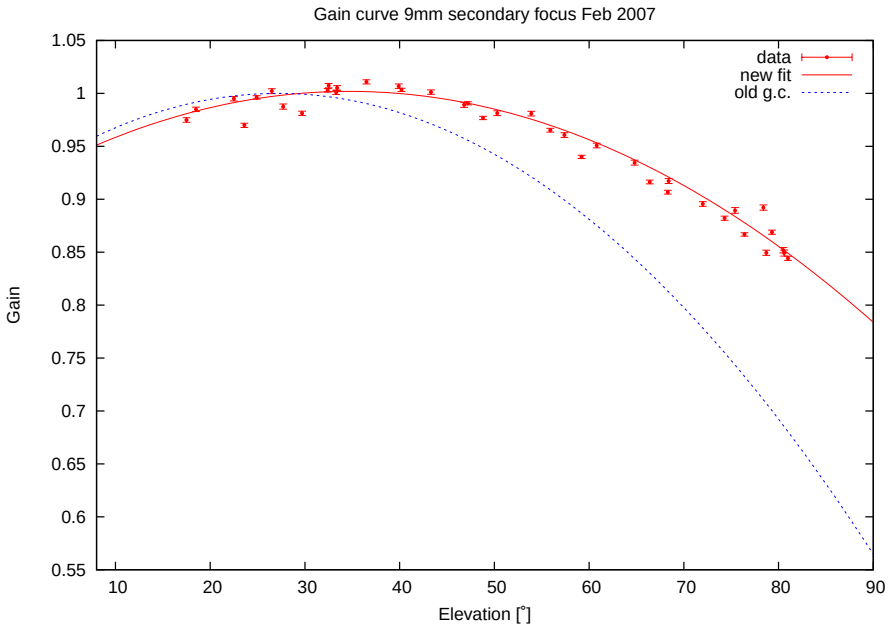

Figure C.9: Old and new gain curve at 9mm.

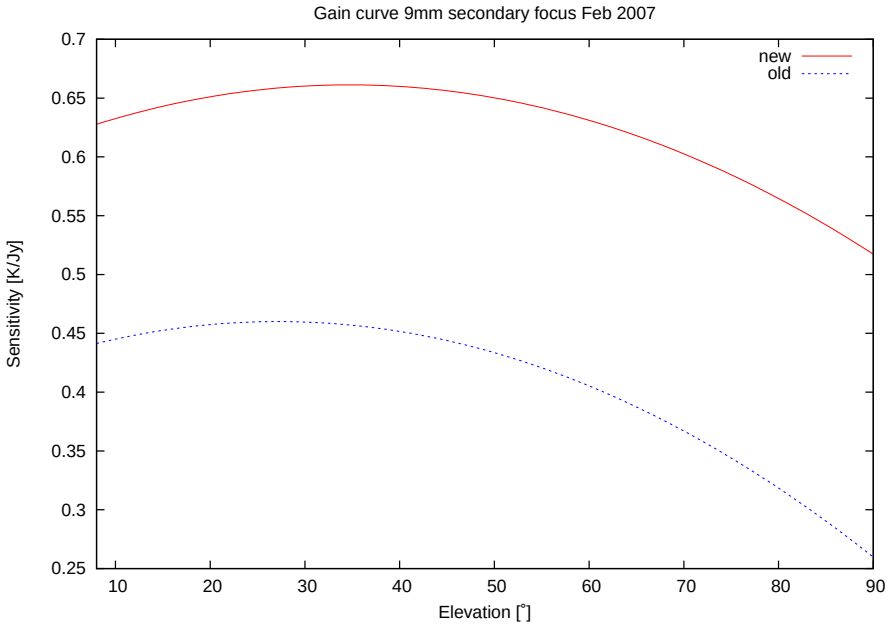

Figure C.10: Old and new sensitivity at 9mm.

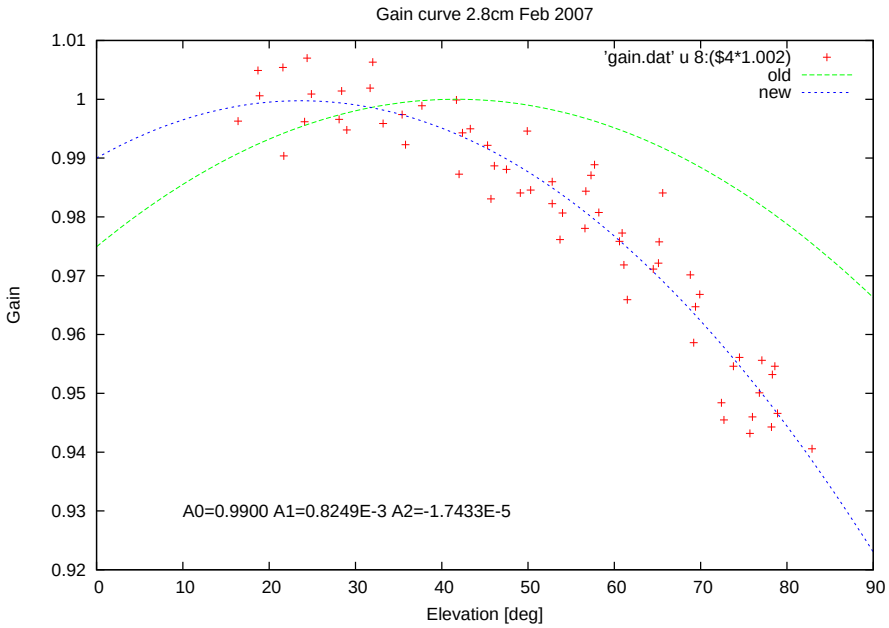

Figure C.11: Old and new gain curve at 2.8cm.

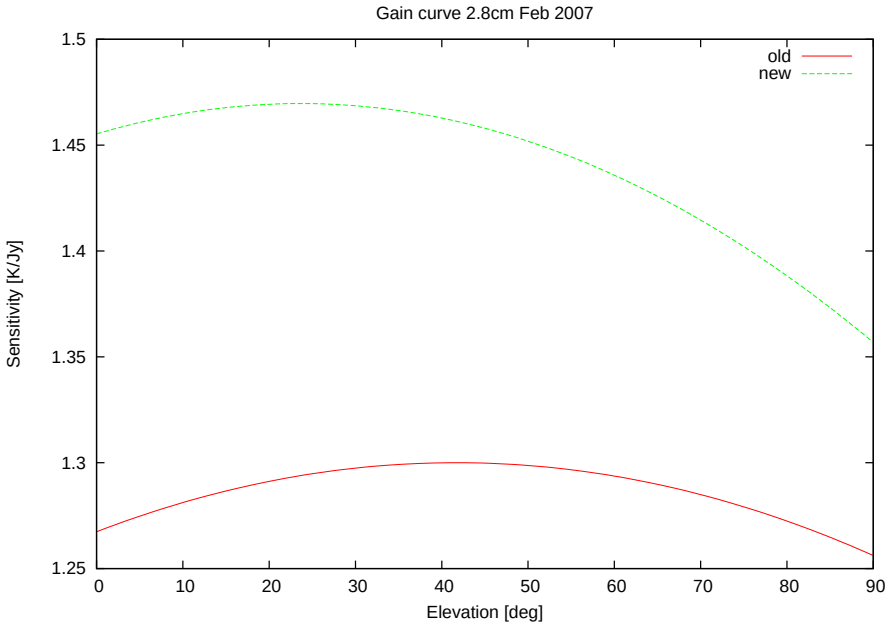

Figure C.12: Old and new sensitivity at 2.8cm.